JOURNAL OF GUIDANCE, CONTROL, AND DYNAMICS
Vol. 30, No. 2, March–April 2007

Angles-Only Orbit Updates for Low-Earth-Orbit Satellites

Chris Sabol*
Air Force Research Lab, Kihei, Hawaii 96753
Kyle T. Alfriend†
Texas A&M University, College Station, Texas 77843-3141
and
David Wiese‡
University of Colorado, Boulder, Colorado 80309

DOI: 10.2514/1.25008

This paper provides the development of a simplified covariance model for predicting the along-track error uncertainty and error uncertainty growth rate for the single-pass, angles-only orbit update, the validation of the model using simulation and real data cases, and a summary of efforts made to characterize the uncertainty of general-perturbations-based element sets. The analysis shows that one of the limiting factors in obtaining a high-accuracy orbit update from a single pass of angles-only data is the eccentricity uncertainty. For the observation characteristics considered, a high-accuracy orbit update could not be obtained if the initial eccentricity uncertainty is 10^{-5} or greater. Analysis of general perturbation element set uncertainties showed that typically the eccentricity uncertainty is no smaller than 10^{-5}, so the eccentricity uncertainty is a limiting factor in obtaining an accurate orbit update with a single pass of angles-only data with general perturbations element sets.

Nomenclature

a	=	semimajor axis
d	=	drift rate
$\mathcal{E}$	=	expectation operator
e	=	eccentricity
$\boldsymbol{e}$	=	orbital element vector
H	=	observation partials matrix
i	=	orbit inclination
J	=	Jacobian
J_2	=	Earth oblateness coefficient
M	=	mean anomaly
N	=	number of observations
$\mathcal{N}$	=	Gaussian distribution
n	=	mean motion
p	=	semilatus rectum
q_1	=	nonsingular element $e\cos\omega$
q_2	=	nonsingular element $e\sin\omega$
P	=	covariance
P_0	=	a priori covariance propagated to current epoch
R	=	orbit radius of truth orbit
$\boldsymbol{R}$	=	measurement noise matrix
R_s	=	radius to sensor site
$T_{\boldsymbol{xe}}$	=	transformation from state vector to differential orbital elements
$\boldsymbol{x}$	=	state vector
$\boldsymbol{y}$	=	measurement vector
W	=	measurement weight matrix
α	=	satellite elevation angle from sensor
Δ	=	time between observations
θ	=	argument of latitude of truth orbit
$\boldsymbol{v}$	=	Gaussian measurement white noise
ρ	=	sensor to satellite range
ρ_{12}	=	correlation coefficient for q_1 and q_2
σ	=	standard deviation
σ_1, σ_2	=	standard deviations of q_1 and q_2
Φ	=	state transition matrix
Ω	=	right ascension
ω	=	argument of perigee

Received 6 May 2006; accepted for publication 29 September 2006.

*Research Aerospace Engineer, U.S. Air Force Research Laboratory Maui Optical and Supercomputing. Member AIAA.

†TEES Distinguished Research Chair Professor, Department of Aerospace Engineering. Fellow AIAA

‡Graduate Student, Department of Aerospace Engineering. Student Member AIAA.

I. Introduction

OVER the past few decades, optical tracking has typically been associated with deep space surveillance and radar tracking with low-Earth-orbit (LEO) space surveillance. However, if one considers the nature of orbit prediction errors and that of optical observation types, optical data can be quite valuable in the orbit update process. Orbit prediction error manifests itself chiefly as along-track runoff and along-track and cross-track periodics. Optical tracking data provide almost direct measurements of the satellite position in the along-track and cross-track directions; thus, these errors can be significantly reduced using optical data estimation techniques. Because along-track error is coupled with radial error, one can also get an indirect estimate of object altitude given a sufficient observation arc and accurate angles data.

Previous work has shown that accurate orbit updates can be performed with one pass of high-accuracy angles-only data [1,2]. Sabol et al. [1] showed that the error from an orbit produced from a general perturbations-based element set can be reduced by an order of magnitude using real data, whereas Alfriend et al. [2] predicted these results in terms of semimajor axis uncertainty using a simplified covariance model. The limitation to this approach is that the orbit update requires an initial covariance matrix corresponding to the uncertainty of the initial conditions. Sabol found desirable initial covariance values through trial and error, comparing orbit update results against a satellite laser ranging-based reference orbit until a coarsely optimal solution was found. Although these efforts showed the promise of orbit updates using angles-only observations, it was not practical because the determination of the initial covariance information was dependent on knowledge of the reference orbit and not reproducible for an arbitrary case.

This paper explores the practical limitations of single-pass, angles-only orbit updates. General perturbations-based element sets are compared against satellite laser ranging-based orbits and against

each other to determine their uncertainty. This information, along with high-accuracy optical tracking data, is used to generate orbit updates. The results are then compared to the satellite laser ranging-based reference orbits to determine the effectiveness of the orbit update.

This paper provides the development of a simplified covariance model for predicting the along-track error uncertainty and error uncertainty growth rate for the single-pass, angles-only orbit update, the validation of that model using simulation and real data cases, and conclusions on the practical expectations of the single-pass, angles-only orbit update.

II. Simplified Covariance Model For Uncertainty Prediction

Assume a satellite is in a circular orbit of radius R and altitude h as shown in Fig. 1, and conditions at epoch are denoted by the subscript 0. The covariance at epoch due to the previous orbit update is P_0. Observations will be equally spaced at intervals of Δ. The planar form of Hill's or the Clohessy–Wiltshire [3] equations in curvilinear coordinates are used as the dynamic model; therefore, the state is

$$\boldsymbol{x}^T = (\delta R/R, \delta R'/\delta\theta, \delta\theta') \tag{1}$$

where the prime denotes differentiation with respect to the true anomaly and δ denotes the difference or error in the state. The state transition matrix is

$$\Phi(\psi) = \begin{pmatrix} 4-3\cos\psi & \sin\psi & 0 & 2(1-\cos\psi) \\ 3\sin\psi & \cos\psi & 0 & 2\sin\psi \\ 6(\sin\psi-\psi) & 2(\cos\psi-1) & 1 & 4\sin\psi-3\psi \\ 6(\cos\psi-1) & -2\sin\psi & 0 & 4\cos\psi-3 \end{pmatrix} \tag{2}$$

$$\psi = n(t-t_0)$$

The measurement equation is

$$\boldsymbol{y} = H\boldsymbol{x} + \boldsymbol{v}, \qquad \boldsymbol{v} = \mathcal{N}(0, \boldsymbol{R}) \tag{3}$$

The covariance at epoch from the batch least squares is

$$P = (A^T W A), \qquad A = \frac{\partial \boldsymbol{y}}{\partial \boldsymbol{x}_0} \tag{4}$$

where the weighting matrix W is usually selected as the inverse of the observation errors, i.e., $W = \boldsymbol{R}^{-1}$. For each observation we get

$$A = \frac{\partial \boldsymbol{y}}{\partial \boldsymbol{x}_0} = \frac{\partial \boldsymbol{y}}{\partial \boldsymbol{x}}\frac{\partial \boldsymbol{x}}{\partial \boldsymbol{x}_0} = H\Phi \tag{5}$$

The inverse of the covariance is

$$A^T W A = \begin{pmatrix} \Phi_0^T H_0^T & \Phi_1^T H_1^T & \cdots & \Phi_N^T H_N^T \end{pmatrix} \begin{pmatrix} W & 0 & \cdots & 0 \\ 0 & W & 0 & 0 \\ \vdots & 0 & \ddots & 0 \\ 0 & 0 & 0 & W \end{pmatrix} \begin{pmatrix} H_0\Phi_0 \\ H_1\Phi_1 \\ \vdots \\ H_N\Phi_N \end{pmatrix}$$

$$A^T W A = \sum_{k=0}^{N-1} \Phi_k^T H_k^T W H_k \Phi_k \tag{6}$$

where

$$\Phi_k = \Phi(t_k - t_0) \tag{7}$$

The estimated state from the previous orbit update propagated to epoch is treated as an observation at epoch and the associated covariance in the rotating Hill frame is the weighting matrix. The covariance at epoch is

$$P = \left[P_0^{-1} + \sum_{k=0}^{N-1} \Phi_k^T H_k^T W H_k \Phi_k \right]^{-1} \tag{8}$$

An important element of this analysis is the covariance of the initial state vector at the beginning of the new set of measurements. This is a function of the state covariance at the previous observation and the propagation time. Rather than selecting arbitrary, but reasonable values, a covariance of orbital elements at the last observation time of the previous track is propagated and transformed to the Hill frame. Gim and Alfriend [4] provide the transformation from nonsingular orbital element space, $\delta\boldsymbol{e}^T = (\delta a, \delta\theta, \delta q_1, \delta q_2)$, to the Hill frame for an elliptic reference orbit. Modifying this result for a circular orbit and the fact that this paper uses the dimensionless variables given in Eq. (1), the transformation is

$$\boldsymbol{x} = T_{\boldsymbol{xe}}\delta\boldsymbol{e} \qquad T_{\boldsymbol{xe}} = \begin{pmatrix} 1/R & 0 & -\cos n\tau & -\sin n\tau \\ 0 & 0 & \sin n\tau & -\cos n\tau \\ 0 & 1 & 0 & 0 \\ -1.5/R & 0 & 2\cos n\tau & 2\sin n\tau \end{pmatrix} \tag{9}$$

The covariance in orbital element space propagates according to

$$P_{\delta\boldsymbol{e}} = \Phi_{\delta\boldsymbol{e}} P_{\delta\boldsymbol{e}0} \Phi_{\delta\boldsymbol{e}}^T$$

$$\Phi_{\delta\boldsymbol{e}} = \begin{pmatrix} 1 & 0 & 0 & 0 \\ -1.5n\tau/R & 1 & 2\sin n\tau & 2(1-\cos n\tau) \\ 0 & 0 & 1 & 0 \\ 0 & 0 & 0 & 1 \end{pmatrix} \tag{10}$$

where τ is the propagation time. In summary, select the baseline initial orbital element covariance $P_{\delta e0}$ and propagate it to epoch using Eq. (10). Then transform it into the Hill frame using

$$P_o = T_{\boldsymbol{xe}} P_{\delta\boldsymbol{e}} T_{\boldsymbol{xe}}^T \tag{11}$$

The other component to the covariance analysis is the measurement equation and partial derivatives. Referring to Fig. 1, the angular measurement is the elevation angle α. Note that the elevation has the range from 0 to π with the angle measured from the horizon in the direction of motion. The model requires the partial derivatives of this angle with respect to the state. The measurement equations are

$$\rho^2 = R^2 + R_e^2 - 2RR_e\cos\theta \qquad \cos\alpha = \left(\frac{R}{\rho}\right)\sin\theta \tag{12}$$

The convention used in the model implementation is to let θ be negative until the satellite is directly over the sensor (nadir) and positive thereafter. Therefore, $\alpha > \pi/2$ when $\theta < 0$. From Eq. (12), the measurement partial derivatives are

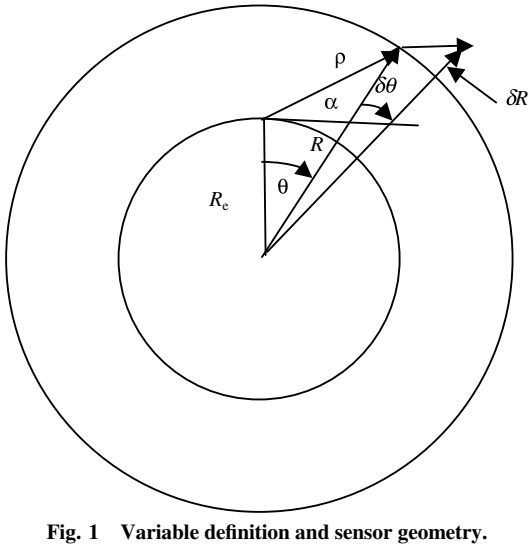

Fig. 1 Variable definition and sensor geometry.

$$\frac{\partial\alpha}{\partial R}=\frac{\sin\theta}{\rho\sin\alpha}\left[\left(\frac{R^2}{\rho^2}\right)\left(1-\frac{R_e}{R}\cos\theta\right)-1\right]$$
$$\frac{\partial\alpha}{\partial\theta}=\left(\frac{R}{\rho\sin\alpha}\right)\left[\left(\frac{RR_e}{\rho^2}\right)\sin^2\theta-\cos\theta\right] \tag{13}$$

For the measurement partials matrix H these partial derivatives are evaluated on the truth orbit. The preceding set of equations allows one to calculate a covariance matrix given the orbit radius R, the initial covariance $P_{\delta e0}$, the propagation time τ, the number of optical observations N, the sensor error statistics (input into W), and the time between observations Δ. For a given orbit, initial covariance, and propagation time, along with sensor error statistics, one can compute quantities such as the along-track position uncertainty as a function of time. Through further calculations, one can formulate the semimajor axis and eccentricity uncertainties, which predict the along-track drift rate and periodic errors, respectively. Keep in mind, this is a simple two-dimensional model and no out-of-plane motion is considered.

The performance metrics used are the in-track error y and the drift rate d in meters per orbit, which is given by

$$d=3\pi\delta a \qquad \delta a=(4\delta R+2R\delta\dot{\theta}/n)=R(4\delta R+2R\delta\theta') \tag{14}$$

The standard deviations of the metrics are

$$\sigma_y=RP_{33}^{1/2} \qquad \sigma_d=3\pi\sigma_{\delta a}=6\pi R(4P_{11}+P_{44}+4P_{14})^{1/2} \tag{15}$$

Determining the eccentricity uncertainty when using the nonsingular elements chosen here is not a straightforward process when $e=0$. The transformation $(q_1,q_2)\rightarrow(e,\omega)$ is equivalent to the transformation from Cartesian to polar coordinates. From Papoulis [5],

$$f(e,\omega)=f(q_1,q_2)/|J_{e,w}|$$
$$J_{e,w}=\frac{\partial(e,\omega)}{\partial(q_1,q_2)}=\begin{pmatrix}q_1/e & q_2/e\\ -q_2/e^2 & q_1/e^2\end{pmatrix} \qquad |J_{e,\omega}|=\frac{1}{e} \tag{16}$$

Assuming a Gaussian joint density function for (q_1,q_2) the joint probability distribution function for the eccentricity and argument of perigee is

$$f(e,\omega)=\frac{e}{2\pi\sigma_1\sigma_2\left(1-\rho_{12}^2\right)^{1/2}}\exp\left\{\left[-\frac{\left(\sigma_1^2+\sigma_2^2\right)e^2}{4(1-\rho_{12}^2)\sigma_1^2\sigma_2^2}\right]\times\left[1+\frac{\left(\sigma_2^2-\sigma_1^2\right)}{\left(\sigma_1^2+\sigma_2^2\right)}\cos 2\omega-\frac{2\rho_{12}\sigma_1\sigma_2}{\left(\sigma_1^2+\sigma_2^2\right)}\sin 2\omega\right]\right\} \tag{17}$$

The eccentricity probability distribution function is given by

$$f(e)=\int_{-\pi}^{\pi}f(e,\omega)\,\mathrm{d}\omega \tag{18}$$

This involves the integration of the second term in the exponential in Eq. (17). This is a complex integration and a closed-form solution is not evident. First note that when $\sigma_1=\sigma_2=\bar{\sigma}$, $\rho_{12}=0$.

$$\int_{-\pi}^{\pi}\exp\left\{-\frac{e^2}{4\left(1-\rho_{12}^2\right)\sigma_1^2\sigma_2^2}\left[\left(\sigma_2^2-\sigma_1^2\right)\cos 2\omega-2\rho_{12}\sigma_1\sigma_2\sin 2\omega\right]\right\}\mathrm{d}\omega=\int_{-\pi}^{\pi}\exp\{0\}\,\mathrm{d}\omega=2\pi \tag{19}$$

Then

$$f(e)=\frac{1}{\bar{\sigma}}\exp\left[-\frac{e^2}{2\bar{\sigma}^2}\right] \tag{20}$$

This is a Rayleigh distribution. Thus, in the general case the eccentricity probability distribution function is a modified Rayleigh distribution. The eccentricity variance is given by

$$\sigma_e^2=\mathcal{E}(e^2)-[\mathcal{E}(e)]^2 \qquad \mathcal{E}(e^n)=\int_0^{\infty}e^n f(e)\,\mathrm{d}e \tag{21}$$

Now consider each of the terms.

$$\mathcal{E}\,(e^2)=\mathcal{E}\left(q_1^2+q_2^2\right)=\sigma_1^2+\sigma_2^2 \tag{22}$$

$$\bar{e}=\mathcal{E}(e) \qquad \bar{e}=\int_0^{\infty}ef(e)\,\mathrm{d}e=\int_0^{\infty}e\int_{-\pi}^{\pi}f(e,\omega)\,\mathrm{d}\omega\,\mathrm{d}e$$
$$\bar{e}=\int_0^{\infty}ef(e)\,\mathrm{d}e$$
$$=\frac{1}{2\pi\sigma_1\sigma_2\left(1-\rho_{12}^2\right)^{1/2}}\int_0^{\infty}e^2\int_{-\pi}^{\pi}\exp\left[-\frac{e^2}{2\tilde{\sigma}^2}\right]\mathrm{d}\omega\,\mathrm{d}e \tag{23}$$

$$\tilde{\sigma}^2=\frac{2\sigma_1^2\sigma_2^2\left(1-\rho_{12}^2\right)}{(\sigma_1^2+\sigma_2^2)}\left[1+\frac{\left(\sigma_2^2-\sigma_1^2\right)}{\left(\sigma_1^2+\sigma_2^2\right)}\cos 2\omega-\frac{2\rho_{12}\sigma_1\sigma_2}{\left(\sigma_1^2+\sigma_2^2\right)}\sin 2\omega\right]^{-1} \tag{24}$$

First, consider again the case when $\sigma_1=\sigma_2=\bar{\sigma}$, $\rho_{12}=0$.

$$\bar{e}=\frac{1}{2\pi\bar{\sigma}^2}\int_0^{\infty}\int_{-\pi}^{\pi}e^2\exp\left(-\frac{e^2}{2\bar{\sigma}^2}\right)\mathrm{d}e\,\mathrm{d}\omega$$
$$\bar{e}=\frac{1}{\bar{\sigma}^2}\int_0^{\infty}e^2\exp\left(-\frac{e^2}{2\bar{\sigma}^2}\right)\mathrm{d}e=\sqrt{\frac{\pi}{2}}\bar{\sigma} \qquad \bar{e}=\left(2-\frac{\pi}{2}\right)\bar{\sigma}^2 \tag{25}$$

Thus, if one starts with $\sigma_1=\sigma_2=\bar{\sigma}$, $\rho_{12}=0$, Eq. (26) can be used to obtain the initial value of $\bar{\sigma}$ given the desired initial σ_e, or vice versa.

Returning to Eq. (17), the integral over ω cannot be obtained in closed form. It can be integrated with respect to e, however.

$$\int_0^{\infty}e^2\exp\left(-\frac{e^2}{2\tilde{\sigma}^2}\right)\mathrm{d}e=\sqrt{\frac{\pi}{2}}\tilde{\sigma}^3 \tag{26}$$

$$\bar{e}=\frac{1}{2\pi(1-\rho_{12})^{1/2}}\sqrt{\frac{\pi}{2}}\int_{-\pi}^{\pi}\tilde{\sigma}^3\,\mathrm{d}\omega \qquad \bar{e}=\frac{2\sigma_1^2\sigma_2^2(1-\rho_{12}^2)\sqrt{\pi}A}{\left(\sigma_1^2+\sigma_2^2\right)^{3/2}}$$
$$A=\frac{1}{2\pi}\int_{-\pi}^{\pi}\left[1+\frac{\left(\sigma_2^2-\sigma_1^2\right)}{\left(\sigma_1^2+\sigma_2^2\right)}\cos 2\omega-\frac{2\rho_{12}\sigma_1\sigma_2}{\left(\sigma_1^2+\sigma_2^2\right)}\sin 2\omega\right]^{-3/2}\mathrm{d}\omega \tag{27}$$

No closed-form solution for A could be found. Therefore, numerical integration was used.

Table 1 Simulation scenario

	Value	Standard deviation
Semimajor axis	7160 km	4.1 m
Eccentricity	0.0001	10^{-6}
Argument of latitude	0 rad	10^{-6} rad
Angular observation	150–30 deg., every 12 s (28 obs over 5.4 min)	5 arcsec

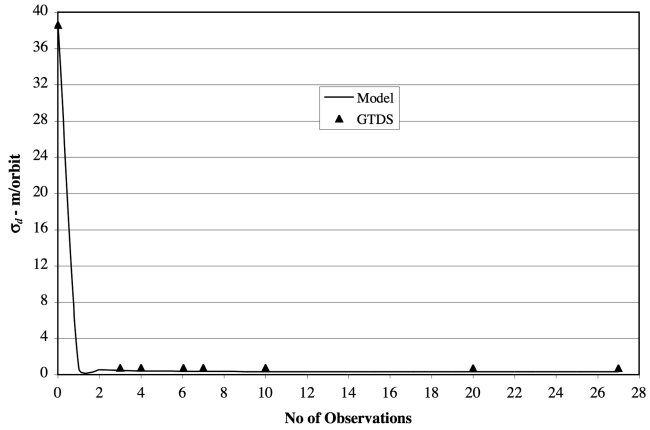

Fig. 2 Simulation along-track drift-rate uncertainty.

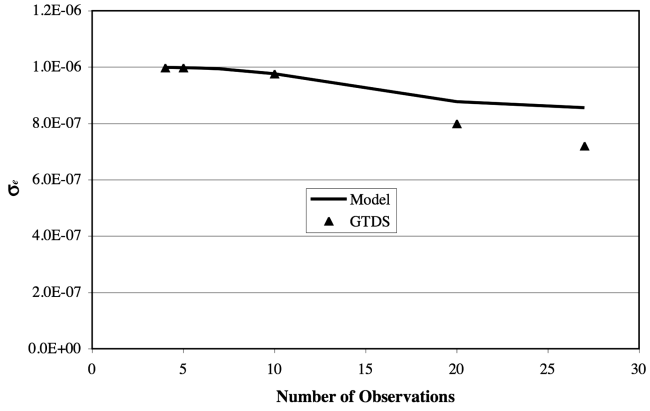

Fig. 3 Simulation eccentricity uncertainty.

III. Validation of the Simplified Covariance Model via Simulation

The uncertainty prediction model was validated through simulation where the assumptions inherent to the model could be tested. This was performed using the Draper Research and Development version of the Goddard Trajectory Determination System (GTDS) [6]. The simulation scenario assumed the conditions listed in Table 1. Angular observation characteristics were chosen based on experience with Maui Space Surveillance Site data [7]. The values in Table 1 were input into the simplified covariance model, and output along-track drift rate and eccentricity uncertainty were recorded at various points throughout the observation span. A simulation scenario was generated in GTDS with the same initial conditions, two-body dynamics and an overhead pass, and the output solution covariance information was recorded. Equation (15) was used to map the GTDS semimajor axis output standard deviation to the along-track drift rate. Figures 2 and 3 compare the results for the along-track drift rate and eccentricity, respectively. For cases without the full data set, the observations were split symmetrically about culmination. From the figures, one can see that the model provides reasonable agreement with the GTDS simulation output.

IV. Orbit Update Trend Analysis

The simplified covariance model was used to explore the impact of the initial uncertainty on the performance of angles-only orbit updates. The performance of the orbit update is dependent on many factors; an interesting coupling exists between the time between orbit updates and the initial semimajor axis, eccentricity, and argument of latitude errors. If the argument of latitude and eccentricity are well known, the semimajor axis can be well estimated given adequate time between the last epoch and observation data to allow sufficient time for the semimajor axis error to generate an along-track error. Eccentricity and argument of latitude uncertainty, however, introduce uncertainty into the semimajor axis estimate because it is difficult for the estimator to differentiate between the three contributors to the along-track error, the semimajor axis error, the eccentricity, and the initial argument of latitude error. Conversely, the estimator has trouble discerning eccentricity and argument of latitude components if the semimajor axis is not well known. These factors are explored in Figs. 4–6. These cases assume the same conditions as the previous cases, which are listed in Table 1. Figure 4 shows the impact of the time between orbit updates [propagation time (PT)] on the orbit update drift rate uncertainty. As the time between updates increases, the more the in-track error due to the semimajor axis error at epoch dominates the total error, with the result that the semimajor axis error is decreased. The effect of the ratio of the in-track error due to the semimajor axis error to the total in-track error at the first observation [error ratio (ER)] is shown in Fig. 5. In Fig. 5, the total along-track uncertainty is 1 km. Because this is statistical, the square root of the sum of the squares of the in-track error due to the initial argument of latitude uncertainty and that due to the semimajor axis uncertainty is the total along-track uncertainty. For example, an initial argument of latitude uncertainty resulting in an initial in-track uncertainty of 600 m and an in-track uncertainty of 800 m resulting from a semimajor axis uncertainty gives a total uncertainty of 1 km, and the error ratio is 0.8. Figure 5 shows that as the initial along-track error becomes dominant, the estimator does a poor job of estimating and correcting the semimajor axis error. The good news is that the initial argument of latitude error should be reasonably small if the initial space surveillance product epoch is near a period of tracking data.

Previous work focused on drift rate as the primary metric of orbit update performance [2]. Although drift rate is a significant component of orbit prediction error, one can easily see that if the drift

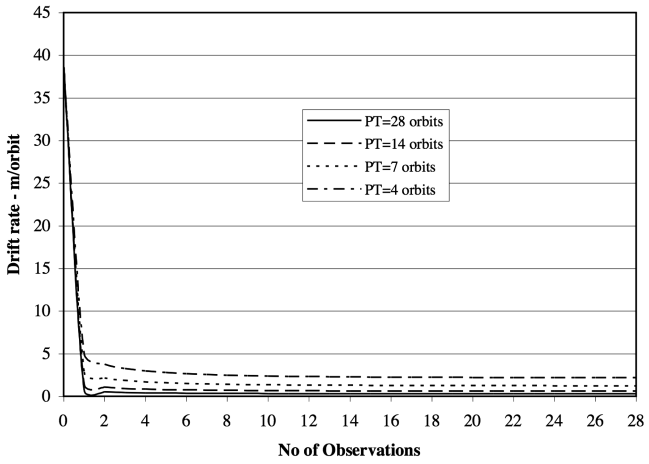

Fig. 4 Effect of time between updates on drift-rate estimate.

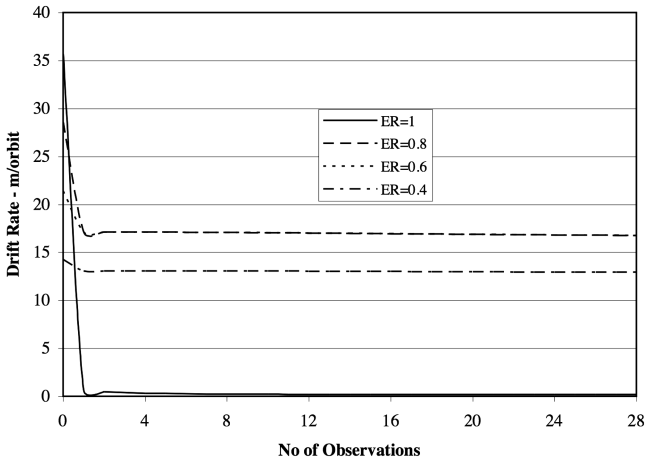

Fig. 5 Effect of initial in-track error magnitude on drift-rate estimate.

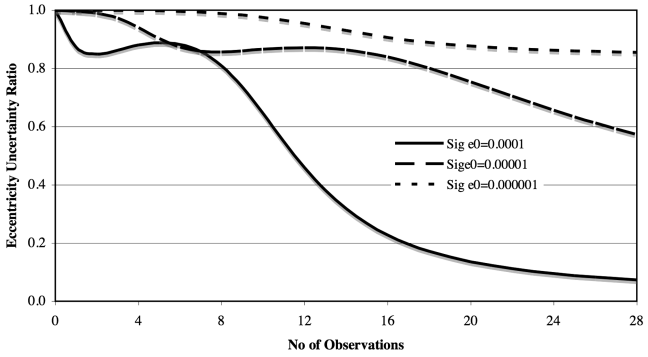

Fig. 6 Normalized eccentricity uncertainty.

rate is on the order of 10 m/orbit, eccentricity errors can be an even larger component of the overall orbit prediction error. The simple covariance model was used to calculate the orbit update eccentricity uncertainty for given initial eccentricity uncertainty.

Again, the scenario considered is described in Table 1 with the exception of the initial eccentricity uncertainty, which was varied. Figure 6 plots the normalized eccentricity uncertainty produced by the model for initial eccentricity uncertainties of 10^{-4}, 10^{-5}, and 10^{-6}; the normalized eccentricity uncertainty is the eccentricity uncertainty divided by the initial uncertainty. Thus, the normalized eccentricity can be thought of as the reduction in the eccentricity uncertainty.

Figure 6 shows that, for the observation characteristics considered, the angles-only orbit update does not improve the eccentricity uncertainty much beyond 10^{-5}. If one starts with excellent eccentricity knowledge, e.g., 10^{-6}, the angles-only orbit update should not significantly change that. If one starts with poor eccentricity knowledge, above 10^{-5}, the angles-only orbit update will improve that knowledge, but probably not much below the 10^{-5} level. Given a semimajor axis of 7160 km, an eccentricity error of 10^{-5} maps into a radial periodic error of ± 72 m and an along-track periodic error of ± 143 m. If one assumes the along-track error is minimal during the observing period and the periodic error is at its trough, which is typically the case, the along-track error 180 deg away from the observing period would be 286 m due to the eccentricity error. This means that initial eccentricity errors not only limit the orbit update performance in terms of drift rate, but may have a major impact on the overall accuracy due to periodic errors as well. Previous work [1] has shown that when the space surveillance product has better eccentricity knowledge, e.g., 10^{-6}, then the angles-only update performs quite well.

V. General Perturbations-Based Element Set Uncertainty

General perturbations-based element sets, such as those contained in CelesTrak,[§] do not come with covariance information. Consistency checks, those comparing orbit propagations to neighboring orbit fits, provide a reasonable indication of the orbit uncertainty. Several studies have used these methods to construct statistical representations of orbit error for given satellites or classes of satellites. Peterson et al. [8], Snow and Kaya [9], and Deguine et al. [10] performed accuracy assessments of Air Force Space Command (AFSPC) two-line element sets (elsets) using these techniques, whereas Jones and Beckerman [11] did a similar analysis of special perturbations vectors generated with Space Surveillance Network data. None of these efforts focused on the orbital elements, however. A similar consistency-check method is implemented here with the goal of producing Keplerian element variance information for any given satellite

Data for these test cases came from publicly available element sets, e.g., CelesTrak[§]. For a given satellite case, element sets were retrieved for a two-week period before the epoch of interest. If this

[§]www.celestrak.com

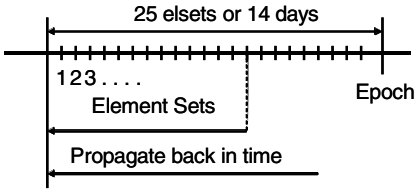

Fig. 7 Consistency-check comparisons for general perturbations-based element sets.

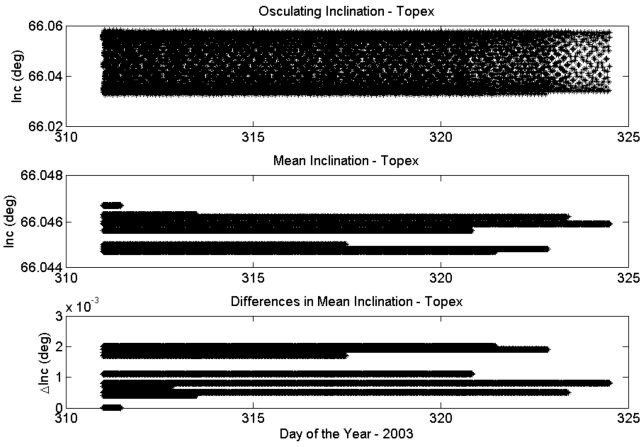

Fig. 8 Effects of converting to mean element space.

14-day span contained more than 25 element sets, only the most recent 25 element sets were used. This was done to minimize propagation error, while trying to maximize the amount of information accrued. Each element set was then propagated backwards in time, to the first day in the set of 25 element sets. Ephemeris output was generated in time steps of ten minutes. Figure 7 illustrates this timeline. At each time step, the osculating position and velocity information were converted to osculating Keplerian elements. Next, the J_2 short periodic effects were removed to form mean Keplerian elements [12]. This step was necessary to separate changes in the slowly varying elements from those due to argument of latitude differences. Figure 8 illustrates the magnitude of the J_2 short periodic effects on the inclination of the TOPEX satellite and how they mask the mean element differences. If one were differencing the inclination values in osculating space, one could see variations on the order of 0.02 deg. These differences, however, are really due to true longitude differences and their impact on the J_2 short periodics. If one compares the mean inclinations as shown in the middle and lower plots of Fig. 8, one can see true inclination differences on the order of 0.002 deg.

The mean orbital elements for each separate orbit were then compared and differenced against a chosen reference orbit, usually the epoch element set. The variance values for each separate Keplerian orbital element were then generated by taking the standard deviation of each set of differences. Outliers were also removed from the data sets to give more realistic uncertainty values. Outliers were defined as data points whose differences were greater than five times the median difference of the full data set.

One can question the meaning of the statistical terms in cases where the underlying assumptions of the data distributions are not necessarily valid; however, this was always meant as an empirical approach and by no means claimed to be rigorous or theoretically correct. As with the previous works, it is an approach that appears to have value despite the limitations of its foundation.

To validate this approach, five test cases were considered. For each test case, the general perturbations-based element set was propagated forward and compared to a satellite laser ranging (SLR) derived reference orbit of much higher accuracy. This provided an independent measure of the element set error. Because the orbit update process is special perturbations-based, the mean elements of

Table 2 Test satellite orbit characteristics

Satellite	Altitude	Eccentricity	Inclination	Epoch
TOPEX	1337 km	0.00083	66 deg	04/09/02, 11/20/03
Lageos 2	5765 km	0.01373	53 deg	11/17/01,
Stella	800 km	0.00075	98 deg	04/09/02
ERS-2	790 km	0.00007	99 deg	11/22/01

Table 3 GTDS DC configuration summary

Integrator	12th-order summed Cowell/Adams predict-partial correct
Step size	60 s
Geopotential	50 × 50 JGM2
Atmospheric drag	Jacchia-Roberts, single Cd
Third body	Solar/lunar point masses based on JPL DE ephemerides
Solar radiation pressure	Single Cr

the general perturbations-based element set were converted to an osculating set via a precise conversion of elements (PCE). The PCE consisted of an initial propagation of the general perturbations-based element set followed by a differential correction to the resulting ephemeris using the special perturbation theory. This produces the best special perturbations-based representation of the general perturbations-based element set. Because the PCE output is used to initialize the orbit update process, the PCE results were also propagated forward and compared to the SLR-derived reference orbit to provide a measure of error. The uncertainties derived from the consistency checks were then compared to the errors in the general perturbations-based element set and PCE output.

For orbit determination studies, it is always desirable to have a "truth" or reference orbit for comparison to assess performance. The international SLR community provides observation data sets to build such reference orbits for a variety of satellites. TOPEX (Satellite Catalog No. 22076), Lageos-2 (22195), Stella (22824), and ERS-2 (23560) were chosen as test cases for this work; TOPEX was used twice. Table 2 contains the approximate altitude, eccentricity, and inclination for each of these satellites; all satellites are in near circular orbits. Reference orbits were constructed for these satellites by performing fits to SLR data available through the NASA Crustal Dynamics Data Information System ftp server.[¶] Analysis indicated that these reference orbits were typically accurate to below 20 m.

GTDS was used to perform the analysis. The GTDS ephemeris generation program was used to propagate the general perturbations-based element sets using an unofficial version of SGP4 [13]. The GTDS Differential Correction (DC) program was used to establish the reference orbit and the fit to the general perturbations-based trajectory for the PCE. The DC program consists of a weighted batch least-squares algorithm, which minimizes the residual differences between the computed and measured quantities over a period of time. Table 3 summarizes the standard GTDS configuration used in the runs. For the PCE, solar radiation pressure was not modeled. Finally, the GTDS ephemeris comparison program was used to compare the general perturbations-based trajectory and the PCE trajectory to the SLR-based reference orbit.

This approach was applied to the five test cases. Figure 9 shows example results for the TOPEX satellite for the 2003 epoch. One can see the calculated standard deviation based on the consistency check agrees reasonably well (same order of magnitude) with the observed differences from the SLR reference orbit. The other test cases showed similar levels of agreement. Table 4 contains the PCE differences at epoch and Table 5 contains the calculated standard deviations for all of the cases.

[¶]C. Noll, Crustal Dynamics Data Information System web page, NASA Goddard Flight Center, http://cddisa.gsfc.nasa.gov/ [cited 16 November 2006].

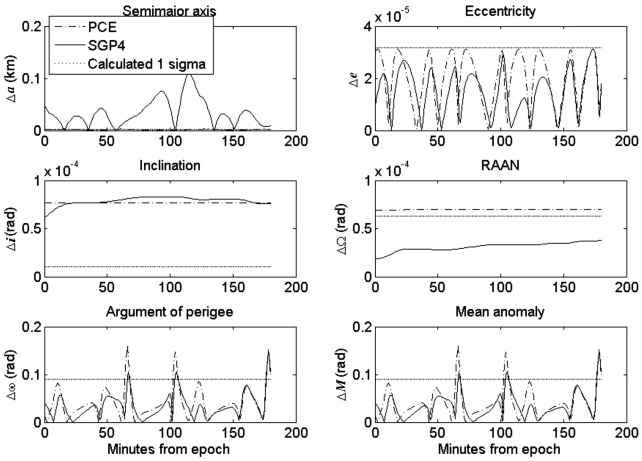

Fig. 9 Element set uncertainty generated for TOPEX 03.

VI. Orbit Update Results

Orbit updates were performed for each of the test cases described in the preceding section. Again, the GTDS DC program was used to generate the orbit update and compare the results against the SLR-based reference orbit over a 24-hour period after the tracking data. PCE-derived osculating Keplerian elements were used as the initial conditions to the estimation process. The DC configuration was identical to what is described in Table 3. The orbital elements were the only parameters estimated in the orbit update; the drag coefficient used in the orbit update was the drag coefficient derived from the PCE. Two DCs were performed for each case: 1) using the PCE differences as the initial uncertainty information, and 2) using the uncertainties calculated by the consistency-check process. These values are contained in Tables 4 and 5, respectively. For all but the Lageos 2 case, a −0.999999 correlation coefficient between the argument of perigee and true anomaly was added to the initial uncertainty values, and the rest of the state was assumed uncorrelated.

The observation data used in this work consisted of azimuth and elevation angles collected from the 3.6 m (AEOS) and 1.6 m telescopes at the Maui Space Surveillance Site (MSSS). Table 6 summarizes the measurements collected for each test case. Data were collected at roughly 10-s intervals over the course of each pass. Accuracy assessment of the data, determined by comparing the observations to the SLR reference orbit, showed it to be of acceptable quality with observation errors usually less than 5 arcseconds [7].

Figure 10 plots the along-track component of the orbit update prediction error for all of the cases using the PCE differences as the initial uncertainty information. Figure 11 contains the same information for the cases using the uncertainty information calculated by consistency checks. In both figures, one can observe the significant periodic errors due to eccentricity errors. Most of the cases have drift rates around 10 m/orbit. Table 7 contains the observed semimajor axis, drift rate, eccentricity, and along-track peak-to-peak periodic errors in the orbit updates for the cases using the consistency-check-based uncertainty.

Comparing Table 7 to Table 5, one can see that four out of the five cases have an improvement from the initial semimajor axis to the orbit update semimajor axis error; three out of the five cases show an order of magnitude improvement. The semimajor axis error maps directly into the orbit prediction drift rate. The final eccentricity errors are on the same order of magnitude as the initial eccentricity uncertainties. These eccentricity errors map into hundreds of meters of along-track periodic errors, which form the major component of the prediction error for many orbits after the orbit update.

In all of the cases, the observed eccentricity error and calculated eccentricity uncertainty were the same order of magnitude, 10^{-5}. This is the area for which the simplified covariance model predicts the angles-only orbit update would have trouble correcting for the eccentricity error. Indeed, the real data validation cases show this to be true. Therefore, it is clear that the eccentricity uncertainty in the

Table 4 Precise conversion of elements differences from SLR reference orbit

Case	a, km	e	i, rad	Ω, rad	ω, rad	M, rad
TOPEX '02	7.0E − 3	3.2E − 5	3.2E − 5	6.3E − 5	6.3E − 2	6.3E − 2
TOPEX '03	1.4E − 3	3.0E − 5	7.7E − 5	7.1E − 5	1.7E − 2	1.7E − 2
Lageos 2	5.5E − 3	5.5E − 5	6.3E − 5	4.5E − 5	2.6E − 4	4.5E − 4
Stella	2.0E − 3	3.2E − 6	3.2E − 5	4.5E − 5	3.2E − 2	3.2E − 2
ERS-2	2.2E − 3	1.0E − 5	1.4E − 5	4.5E − 5	8.9E − 2	8.9E − 2

Table 5 Calculated uncertainties for element sets

Case	a, km	e	i, rad	Ω, rad	ω, rad	M, rad
TOPEX '02	3.2E − 3	1.0E − 5	1.4E − 5	4.5E − 5	5.5E − 2	5.5E − 2
TOPEX '03	2.2E − 3	3.2E − 5	1.0E − 5	6.3E − 5	8.9E − 2	8.9E − 2
Lageos 2	5.5E − 4	1.4E − 5	1.0E − 5	1.7E − 5	7.7E − 4	8.4E − 4
Stella	3.2E − 3	1.0E − 5	1.4E − 5	4.5E − 5	5.5E − 2	5.5E − 2
ERS-2	2.0E − 2	9.0E − 6	1.4E − 5	2.6E − 5	1.4E − 2	1.4E − 2

general perturbations-based element sets used in this analysis is a limiting factor in the practical application of the angles-only orbit update.

All of the analysis contained in this paper focused on the along-track component of motion. It is true that the orbit update will also have cross-track errors that may not be negligible. These errors, however, should be periodic and bounded given adequate force modeling and therefore they are not as large of a concern as the along-track errors, which may grow rapidly with time.

VII. Conclusions

This paper explored the practical limitations of single-pass, angles-only orbit updates. A simplified covariance model was developed to predict the semimajor axis, eccentricity, and argument of latitude uncertainty of an angles-only orbit update. The result of this information was essentially a predicted along-track error uncertainty and error uncertainty growth rate for the orbit update. The model was then used to show the impact of the initial space surveillance product's covariance on the orbit update. The results suggest that, for the observation characteristics considered, a single pass of angles-only data may not be sufficient to produce a high-accuracy orbit update if the initial eccentricity uncertainty is on the order of 10^{-5} or higher.

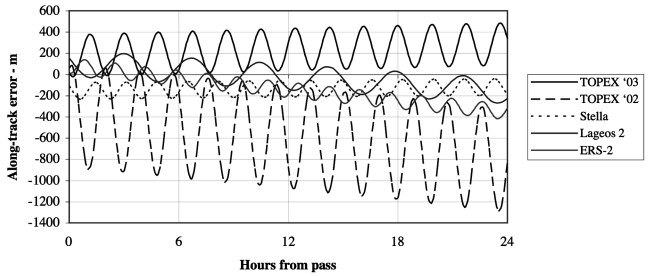

Fig. 10 Orbit update along-track prediction error using PCE differences as the uncertainty.

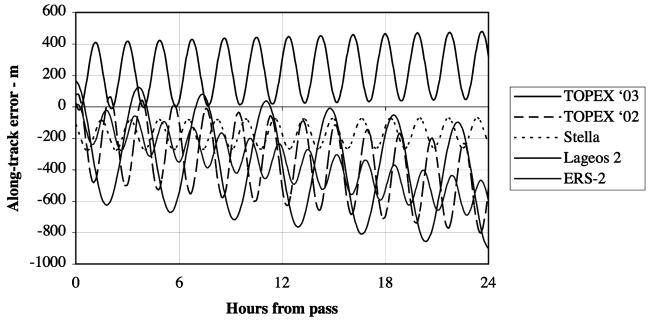

Fig. 11 Orbit update along-track prediction error using calculated uncertainty.

Table 6 Data summary

Satellite	Date	Telescope	Max. elevation	No. of obs pairs
TOPEX '02	11 April 2002	1.6 m	64 deg	55
TOPEX '03	23 Nov. 2003	1.6 m	84 deg	75
Lageos 2	21 Nov. 2001	AEOS	84 deg	32
Stella	13 April 2002	1.6 m	34 deg	9
ERS-2	25 Nov. 2001	AEOS	31 deg	84

Table 7 Orbit update error metrics for calculated uncertainty cases

Case	Semimajor axis error, km	Drift rate, m/orbit	Eccentricity error	Peak-to-peak periodic, m
TOPEX '02	2.5E − 3	−24	1.8E − 5	570
TOPEX '03	−6.0E − 4	6	1.3E − 5	410
Lageos 2	4.6E − 3	−43	1.6E − 5	790
Stella	1.0E − 4	−1	6.7E − 6	190
ERS-2	3.6E − 3	−34	8.7E − 6	250

Several real data cases were examined. Two methods were used to determine the initial uncertainty of general perturbations-based element sets. First, the element sets were compared against satellite laser ranging-based reference orbits to determine their uncertainty. Second, multi-element set consistency checks were performed to empirically approximate their uncertainty. This information, along with high-accuracy optical tracking data, was used to generate orbit updates. The results were then compared to the satellite laser ranging based reference orbits.

The results show that trends in the orbit update uncertainty are predicted by the simplified covariance model. The level of eccentricity uncertainty observed in the general perturbations-based element sets appears to be a limiting factor in the practical application of the single-pass, angles-only orbit update using those space surveillance products. Given a space surveillance product with better eccentricity knowledge, the angles-only orbit update should perform quite well, however.

References

[1] Sabol, C., Luu, K. K., and Alfriend, K. T., "High Accuracy Orbit Updates Using Angles-Only Data," *Advances in the Astronautical Sciences*, Vol. 120, Univelt Publishers, San Diego, CA, 2005,

pp. 1547–1558.
[2] Alfriend, K., Sabol, C., and Luu, K. K., "Comparison of Optical and Radar Tracking For Catalog Maintenance," *Advances in the Astronautical Sciences*, Vol. 120, Univelt Publishers, San Diego, CA, 2005, pp. 1531–1546.
[3] Clohessy, W. H., and Wiltshire, R. S., "Terminal Guidance System for Satellite Rendezvous," *Journal of the Astronautical Sciences*, Vol. 27, No. 9, Sept. 1960, pp. 653–678.
[4] Gim, D.-W., and Alfriend, K. T., "State Transition Matrix of Relative Motion For the Perturbed Noncircular Reference Orbit," *Journal of Guidance, Control, and Dynamics*, Vol. 26, No. 6, Nov.–Dec. 2003, pp. 956–971.
[5] Papoulis, A., *Probability, Random Variables and Stochastic Processes*, McGraw–Hill, New York, 1984, p. 143.
[6] Computer Sciences Corporation and NASA/GSFC Systems Development and Analysis Branch (eds.), *Research and Development Goddard Trajectory Determination System (R&D GTDS) User's Guide*, NASA Goddard Space Flight Center, July 1978.
[7] Shishido, B., Brem, B., Konohia, P., Sabol, C., and Luu, K. K., "Accuracy Assessment of MSSS Metric Tracking Data," AAS Paper 04-191, Feb. 2004.
[8] Peterson, G., Gist, R. G., and Oltregge, D. L., "Covariance Generation for Space Objects Using Public Data," *Advances in the Astronautical Sciences*, Vol. 108, Univelt Publishers, San Diego, CA, 2001, pp. 201–214.
[9] Snow, D., and Kaya, D., "Element Set Prediction Accuracy," *Advances in the Astronautical Sciences*, Vol. 103, Univelt Publishers, San Diego, CA, 2000, pp. 1937–1956.
[10] Deguine, B., Foliard, J., Alby, F., Donath, T., Bouchard, J., and Quillen, C., "Covariance Modeling in Satellite Collision Risk Activities," AIAA Paper 2002-4631, Aug. 2002.
[11] Jones, J., and Beckerman, M., "Determination and Modeling of Error Densities in Ephemeris Prediction," AAS Paper 99-175, Feb. 1999.
[12] Vallado, D., *Fundamentals of Astrodynamics and Applications*, McGraw-Hill, New York, 1997.
[13] Herriges, D. L., "NORAD General Perturbation Theories: An Independent Analysis," M.S. Thesis, Dept. of Aeronautics and Astronautics, MIT, Cambridge, MA, Jan. 1988.